Hexagonally Deformed Fermi Surface of the 3D Topological Insulator Bi$_2$Se$_3$

K. Kuroda,[1] M. Arita,[2] K. Miyamoto,[2] M. Ye,[1] J. Jiang,[1] A. Kimura,[1,*] E. E. Krasovskii,[3,4,5] E. V. Chulkov,[3,4,6] H. Iwasawa,[2] T. Okuda,[2] K. Shimada,[2] Y. Ueda,[7] H. Namatame,[2] and M. Taniguchi[1,†]

[1]*Graduate School of Science, Hiroshima University, 1-3-1 Kagamiyama, Higashi-Hiroshima 739-8526, Japan*
[2]*Hiroshima Synchrotron Radiation Center, Hiroshima University, 2-313 Kagamiyama, Higashi-Hiroshima 739-0046, Japan*
[3]*Departamento de Física de Materiales, Facultad de Ciencias Químicas, Universidad del Pais Vasco/Euskal Herriko Unibertsitatea, Apartado 1072, 20080 San Sebastián/Donostia, Basque Country, Spain*
[4]*Donostia International Physics Center (DIPC),
Paseo Manuel de Lardizabal 4, 20018 San Sebastián/Donostia, Basque Country, Spain*
[5]*IKERBASQUE, Basque Foundation for Science, 48011 Bilbao, Spain*
[6]*Centro de Física de Materiales CFM—Materials Physics Center MPC, Centro Mixto CSIC-UPV/EHU,
Edificio Korta, Avenida de Tolosa 72, 20018 San Sebastián, Spain*
[7]*Kure National College of Technology, Agaminami 2-2-11, Kure 737-8506, Japan*
(Received 10 June 2010; published 10 August 2010)

A hexagonal deformation of the Fermi surface of Bi$_2$Se$_3$ has been for the first time observed by angle-resolved photoemission spectroscopy. This is in contrast to the general belief that Bi$_2$Se$_3$ possesses an ideal Dirac cone. The hexagonal shape is found to disappear near the Dirac node, which would protect the surface state electrons from backscattering. It is also demonstrated that the Fermi energy of naturally electron-doped Bi$_2$Se$_3$ can be tuned by 1% Mg doping in order to realize the quantum topological transport.

After the theoretical prediction and experimental realization of two-dimensional topological insulators in the HgTe/CdTe quantum well [1–4], a spectroscopic discovery of a three-dimensional topological insulator by probing the odd number of massless Dirac cones has generated a great interest in this new state of quantum matter [5–9]. Unlike the conventional Dirac fermions as found in graphene, this novel electronic state possesses helical spin textures protected by time-reversal symmetry, which could realize the quantum spin transport without heat dissipation. This new state of matter has been predicted to exist in a number of materials, for example, in Bi$_{1-x}$Sb$_x$, Bi$_2$Se$_3$, Bi$_2$Te$_3$, and Sb$_2$Te$_3$ [10]. Among them, stoichiometric Bi$_2$Se$_3$ is theoretically predicted to be a 3D topological insulator with a single Dirac cone within a substantial bulk energy gap (0.3 eV), which makes it the most suitable candidate for the high-temperature spintronics application [10]. However, in the actual situation, the bulk conduction band is energetically lowered and crosses the Fermi energy through natural electron doping from vacancies or antisite defects, which allows bulk electron conduction. In order to avoid the bulk electron conduction and realize the quantum spin Hall phase, the Fermi energy must be tuned by additional doping [11,12].

In ideal topological insulators with perfect linear dispersion, the surface state electrons should be protected from backscattering by nonmagnetic impurities between time-reversal partners with opposite momenta because of their opposite spin configurations. However, recent scanning tunneling microscopy experiments for the Bi$_2$Te$_3$ surface show a clear quasiparticle interference pattern as a result of backscattering nearby the step edge or at the point defect on the surface [13,14]. Theoretically, it is pointed out that the hexagonal Fermi surface warping would also induce the quasiparticle interference pattern [15]. It is generally believed that, owing to a large band gap (0.35 eV), which exceeds the thermal excitation energy at room temperature, Bi$_2$Se$_3$ features a nearly ideal Dirac cone, in contrast to Bi$_2$Te$_3$ [16,17]. In the present Letter, we show by a precise angle-resolved photoemission spectroscopy (ARPES) measurement that the Fermi surface of naturally electron-doped Bi$_2$Se$_3$ is hexagonally deformed, while the constant energy contour is circular-shaped near the Dirac point. We also show that the Fermi energy can be effectively tuned by doping the sample with Mg.

Bi$_2$Se$_3$ forms a rhombohedral crystal structure with space group $R\bar{3}m$, which comprises a quintuple Se-Bi-Se-Bi-Se layer as shown in Fig. 1(a). The single crystalline samples of Bi$_{2-x}$Mg$_x$Se$_3$ were grown by a standard procedure using the Bridgman method. Angle-resolved photoemission spectroscopy was performed with the photon energy of 31 eV at the linear undulator beam line (BL1) of Hiroshima Synchrotron Radiation Center. The photoemission spectra were acquired with a hemispherical photoelectron analyzer (VG-SCIENTA R4000) at 10 K, by using linearly polarized light with the electric field vector perpendicular to the plane spanned by the surface normal and photoelectron propagation vector (*s* polarization). The constant energy contours were obtained by changing the azimuthal angle of the sample as shown in Fig. 1(b). The
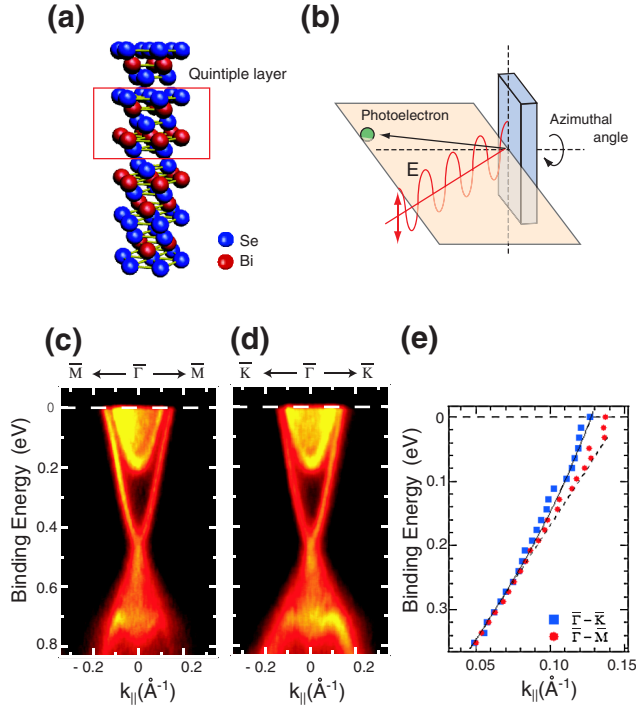
FIG. 1 (color online). (a) Crystal structure of Bi_2Se_3. A quin-tuple layer is indicated by the rectangle. (b) Experimental setup for ARPES measurement. The electric field direction of the incident photon is perpendicular to the plane spanned by the surface normal and photoelectron propagation vector. (c), (d) Experimental energy dispersion curves of Bi_2Se_3 taken along the $\bar{\Gamma}$-$\bar{M}$ and $\bar{\Gamma}$-$\bar{K}$ lines ($h\nu = 31$ eV). (e) Intensity maxima of ARPES spectra along the $\bar{\Gamma}$-$\bar{M}$ and $\bar{\Gamma}$-$\bar{K}$ lines as denoted with boxes and circles, respectively. The solid and dashed lines are a fit with the effective Hamiltonian along the $\bar{\Gamma}$-$\bar{M}$ and $\bar{\Gamma}$-$\bar{K}$ directions, respectively (see text).

overall energy and angular resolutions were set at 15 meV and $\pm 0.1°$, respectively, which enables us to trace very steep Dirac cones. The samples were *in situ* cleaved under the ultrahigh vacuum below 1×10^{-8} Pa.

Figures 1(c) and 1(d) show the energy dispersion curves acquired by ARPES along two different high-symmetry lines, $\bar{\Gamma}$-$\bar{M}$ and $\bar{\Gamma}$-$\bar{K}$ of the surface Brillouin zone, respectively. We find that the surface state bands cross E_F, and these bands intersect at the Dirac point at the binding energy (E_B) of 450 meV. The bulk conduction band is enclosed inside the surface state bands above $E_B = 200$ meV, which is consistent with the previous report [8]. The M-shaped valence band is also recognized below $E_B = 680$ meV. Note that the spectral weight of the bulk conduction band is suppressed when excited with s-polarized light in the present case, while the bulk states dominate the photoemission spectra for p-polarized light in the photon energy range from 21 to 31 eV as found in the previous report [8]. This implies that the experiment with s-polarized light is suitable for the Fermi surface mapping of this surface state. Figure 1(e) presents the intensity

maxima of the surface states along two high-symmetry lines. We find that the energy dispersion along $\bar{\Gamma}$-$\bar{M}$ is almost linear, while along $\bar{\Gamma}$-$\bar{K}$ it is warped toward the smaller $k_\parallel$. The magnitude of the wave vectors at E_F (Fermi wave vector: k_F) can be estimated from these plots to be 0.140 and 0.131 Å^{-1} along the $\bar{\Gamma}$-$\bar{M}$ and $\bar{\Gamma}$-$\bar{K}$ directions, respectively. The different k_F values correlate with the anisotropy of energy dispersions between these high-symmetry lines, which has not been elucidated so far. The anisotropic energy dispersion can be described with the effective Hamiltonian $H(\mathbf{k}) = k^2/2m^* + v(k_x\sigma_y - k_y\sigma_x) + (\lambda/2)(k_+^3 + k_-^3)\sigma_z$, where $k_\pm = k_x \pm k_y$ and v, λ, and σ_z denote the Fermi velocity, warping parameter, and z component of the Pauli matrix, respectively [15]. We find that the experimental dispersions are reproduced well by the calculated ones by using the effective Hamiltonian with the measured Fermi velocity $v = 3.55$ eV $\cdot$ Å and $\lambda = 128$ eV $\cdot$ Å^3 as shown in Fig. 1(e).

According to the energy dispersion shown in Figs. 1(c)–1(e), the Fermi surface topology should also be anisotropic. Figure 2 summarizes two-dimensional slices in k space (-0.15 Å$^{-1} \leq k_x, k_y \leq +0.15$ Å^{-1}) at several energies from the Dirac point to E_F of undoped Bi_2Se_3. The whole set of images has been acquired within two hours in order to avoid an energy shift, which may be caused by the molecular adsorption on the surface [11]. For the present Fermi surface mapping, we used a different sample with a lower defect concentration, resulting in a shallower Dirac point (350 meV from E_F) than that in Fig. 1. At 100 meV, a circular-shaped constant energy contour is clearly identi-fied. In going from the Dirac point towards E_F, the shape of constant energy contour evolves from a circle to a hexagon above 200 meV with increasing Fermi surface area. It is noticed that the shape of the constant energy contour is nearly a circle when the bulk conduction band is absent in the same energy region, but the deformation starts to occur above 200 meV, when the bulk conduction band begins to be enclosed inside the surface constant energy contour as clearly shown in the slices at 250, 300, and 350 meV. The observed hexagonal constant energy contour enclosing the bulk states near E_F follows the crystal symmetry of Bi_2Se_3.

However, the effective Hamiltonian, where the effect of the bulk electronic structure is neglected, is insufficient to gain further insight into the origin of the observed hexago-nal deformation of the Fermi surface. We have performed a first principles calculation of the surface states with a slab of 5 f.u. with a two-component self-consistent full-potential augmented plane wave method [18]. The calcu-lated constant energy contours are shown for 250, 300, 350, and 435 meV relative to the Dirac point in Fig. 2(e). The shape is nearly a circle from zero to 250 meV, and it starts deforming at 300 meV. The theoretical Fermi vector magnitude at 440 meV is 0.142 Å^{-1} in the $\bar{\Gamma}$-$\bar{M}$ direction and 0.118 Å^{-1} in the $\bar{\Gamma}$-$\bar{K}$ direction, which is consistent with the observed values. More important, the electron spin
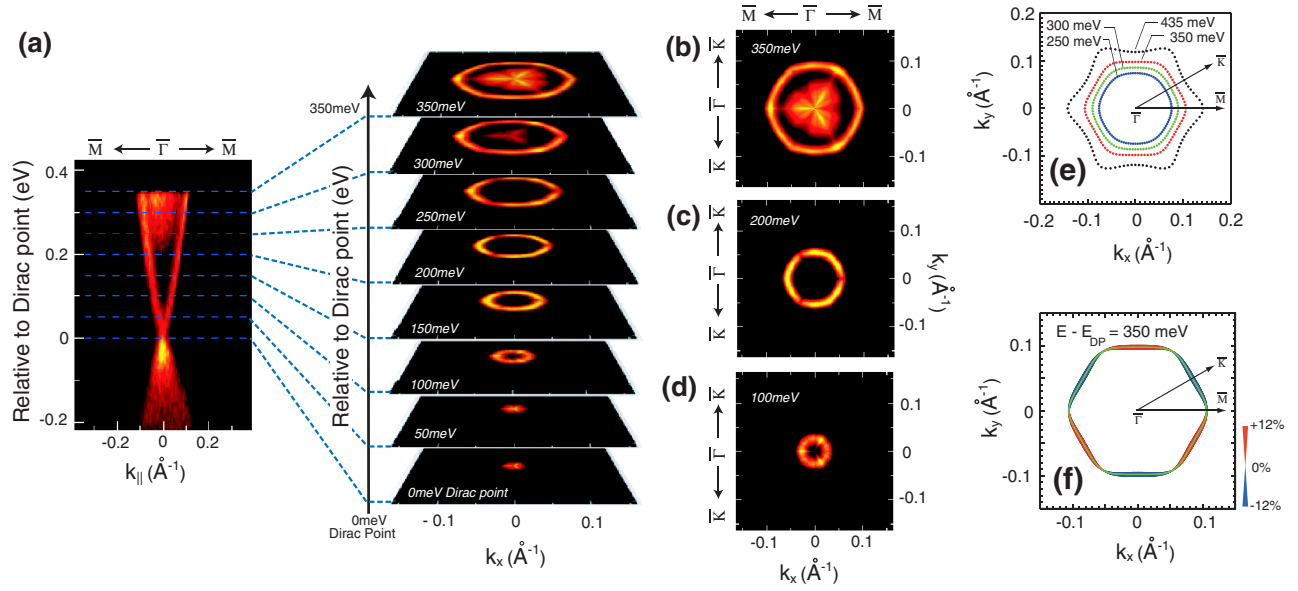
FIG. 2 (color online).   (a) Energy dispersion curve along the $\bar{\Gamma}$-$\bar{M}$ direction (left) and constant energy contours at several energies from 0 (Dirac point) to 350 meV (Fermi surface). Selected constant energy contours at (b) 350, (c) 200, and (d) 100 meV. (e) Calculated constant energy contours at 250, 300, 350, and 435 meV for a slab of 5 f.u. (f) Predicted surface perpendicular projection of spin polarization for the constant energy contour at 350 meV.

acquires a surface perpendicular projection [see Fig. 2(f)] accompanied by the Fermi surface deformation. The out-of-plane spin polarization is maximal in the $\bar{\Gamma}$-$\bar{K}$ direction, where at 350 meV it reaches 12%, and it vanishes in the $\bar{\Gamma}$-$\bar{M}$ line due to the mirror symmetry.

The experimentally discovered hexagonal deformation of the Fermi surface in Bi_2Se_3, which was believed to have an ideal Dirac cone [8], opens a possibility to realize the new quantum phases on the topological insulator surface. On the ideal topological insulator surface with a circular Fermi surface, the formation of a charge density wave or a spin density wave (SDW) is forbidden. Although the hexagonal deformation in Bi_2Se_3 is weaker than in Bi_2Te_3 [9], the two flat segments of hexagonal Fermi surface that face each other with a distance of $2k_F$ along the $\bar{\Gamma}$-$\bar{K}$ direction would lead to a strong nesting and possibly generate a SDW as suggested by Fu [15]. Note that the quasiparticle interference might still be a minor effect in the vicinity of nonmagnetic defects or step edges on the surface because the spin directions at the two flat Fermi surfaces are completely opposite. This is in contrast to the heavily warped Fermi surface in Bi_2Te_3, where the quasiparticle interference is clearly observed in the recent STM experiments [13,14]. However, the present calculation, which reproduces the observed constant energy contours quite well, further predicts that the quasiparticle interference could occur above E_F where the shape of the constant energy contour becomes a hexagram at 435 meV measured from the Dirac point as shown in Fig. 2(e). Since the predicted out-of-plane spin polarization further increases to 17% at 435 meV, the scattering channel could be opened

mainly through the vertical spin component as discussed for the Bi_2Te_3 surface [13,15,19]. Furthermore, in the presence of magnetic impurities, the quasiparticle interference will be allowed and the scattering could be affected by the shape of the Fermi surface. More importantly, since the indirect exchange coupling between the magnetic impurities is mediated by the helical Dirac electrons, we expect that one can control the magnetic order or the spin alignment by tuning the magnitude of the Fermi wave vector (k_F) on the three-dimensional topological insulator surface [20]. Besides, a peculiar magnetic order and a colossal magnetic anisotropy would appear in the presence of the deformed Fermi surface.

In order to realize the quantum topological transport, the Fermi level should be brought into the energy gap by doping with nonmagnetic elements. It also enables us to tune the Fermi vector and the size and shape of the Fermi surface from a hexagon to a circle, associated with electron scattering and magnetic ordering as mentioned above. It should be noted, on the other hand, that the dopants themselves could become a scattering source. Among several scattering factors, a spin-orbit coupling might affect the spin lifetime significantly. As is predicted for Bi_2Te_3 surface, the impurity with a significant spin-orbit coupling could enhance quasiparticle interference especially with large momenta [19]. It may also be expected that the foreign atom doping, which is generally adopted for tuning the topological insulator, could induce the backscattering. To minimize the backscattering originating from spin-orbit coupling, a light element with a negligible spin-orbit coupling should be chosen for the hole doping. In this work,
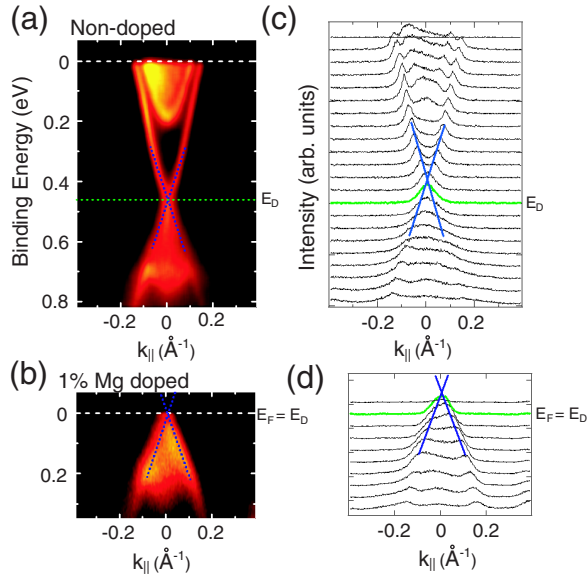
FIG. 3 (color online). Experimental energy dispersion curves of (a) nondoped and (b) 1% Mg-doped Bi_2Se_3 along the $\bar{\Gamma}$-$\bar{M}$ line. (c),(d) Momentum distribution curves for (a) and (b), respectively.

we have tried to realize the hole doping in Bi_2Se_3 with Mg, which is light enough to have negligible spin-orbit coupling.

The ARPES energy dispersion curve along $\bar{\Gamma}$-$\bar{M}$ of Mg-doped Bi_2Se_3 ($Bi_{1.98}Mg_{0.02}Se_3$) is shown in Fig. 3(b). Figure 3(d) exhibits a series of momentum distribution curves in the E_B range of 0–0.3 eV. For comparison, the corresponding dispersion curve of naturally electron-doped Bi_2Se_3 is also depicted in Fig. 3(a) together with momentum distribution curves in Fig. 3(c). One can see that the Dirac point is just located at the Fermi energy by replacing 1% of Bi atoms with Mg. This successful tuning of the carrier density clearly demonstrates that Bi_2Se_3 can be brought into the quantum topological transport regime.

In summary, the hexagonal deformation of the Fermi surface of Bi_2Se_3 has been established by a high-resolution ARPES experiment with s-polarized light. The flat segments facing each other in the hexagonal Fermi surface topology would enable a strong nesting, leading to a new quantum phase such as a SDW. Further Fermi surface deformation can be expected in the unoccupied state, which would generate the quasiparticle interference by a nonmagnetic impurity on the surface. Finally, we have demonstrated that the Fermi energy of naturally electron-doped Bi_2Se_3 can be tuned by 1% Mg doping in order to realize the quantum topological transport.

*akiok@hiroshima-u.ac.jp
†Also at Hiroshima Synchrotron Radiation Center, Hiroshima University, 2-313 Kagamiyama, Higashi-Hiroshima 739-0046, Japan.

[1] C. L. Kane and E. J. Mele, Phys. Rev. Lett. **95**, 146802 (2005).
[2] B. A. Bernevig and S. C. Zhang, Phys. Rev. Lett. **96**, 106802 (2006).
[3] B. A. Bernevig, T. L. Hughes, and S. C. Zhang, Science **314**, 1757 (2006).
[4] M. König, S. Wiedmann, C. Brüne, A. Roth, H. Buhmann, L. W. Molenkamp, X. L. Qi, and S. C. Zhang, Science **318**, 766 (2007).
[5] D. Hsieh, D. Qian, L. Wray, Y. Xia, Y. S. Hor, R. J. Cava, and M. Z. Hasan, Nature (London) **452**, 970 (2008).
[6] D. Hsieh, Y. Xia, L. Wray, D. Qian, A. Pal, J. H. Dil, J. Osterwalder, F. Meier, G. Bihlmayer, C. L. Kane, Y. S. Hor, R. J. Cava, and M. Z. Hasan, Science **323**, 919 (2009).
[7] A. Nishide, A. A. Taskin, Y. Takeichi, T. Okuda, A. Kakizaki, T. Hirahara, K. Nakatsuji, F. Komori, Y. Ando, and I. Matsuda, Phys. Rev. B **81**, 041309 (2010).
[8] Y. Xia, D. Qian, D. Hsieh, L. Wray, A. Pal, H. Lin, A. Bansil, D. Grauer, Y. S. Hor, R. J. Cava, and M. Z. Hasan, Nature Phys. **5**, 398 (2009).
[9] Y. L. Chen, J. G. Analytis, J.-H. Chu, Z. K. Liu, S.-K. Mo, X. L. Qi, H. J. Zhang, D. H. Lu, X. Dai, Z. Fang, S. C. Zhang, I. R. Fisher, Z. Hussain, and Z.-X. Shen, Science **325**, 178 (2009).
[10] H. Zhang, C. X. Liu, X. L. Qi, X. Dai, Z. Fang, and S. C. Zhang, Nature Phys. **5**, 438 (2009).
[11] D. Hsieh, Y. Xia, D. Qian, L. Wray, J. H. Dil, F. Meier, J. Osterwalder, L. Patthey, J. G. Checkelsky, N. P. Ong, A. V. Fedorov, H. Lin, A. Bansil, D. Grauer, Y. S. Hor, R. J. Cava, and M. Z. Hasan, Nature (London) **460**, 1101 (2009).
[12] Y. S. Hor, A. Richardella, P. Roushan, Y. Xia, J. G. Checkelsky, A. Yazdani, M. Z. Hasan, N. P. Ong, and R. J. Cava, Phys. Rev. B **79**, 195208 (2009).
[13] T. Zhang, P. Cheng, X. Chen, J. F. Jia, X. Ma, K. He, L. Wang, H. Zhang, X. Dai, Z. Fang, X. Xie, and Q. K. Xue, Phys. Rev. Lett. **103**, 266803 (2009).
[14] Z. Alpichshev, J. G. Analytis, J.-H. Chu, I. R. Fisher, Y. L. Chen, Z. X. Shen, A. Fang, and A. Kapitulnik, Phys. Rev. Lett. **104**, 016401 (2010).
[15] L. Fu, Phys. Rev. Lett. **103**, 266801 (2009).
[16] E. Mooser and W. B. Pearson, Phys. Rev. **101**, 492 (1956).
[17] J. Black, E. M. Conwell, L. Seigle, and C. W. Spencer, J. Phys. Chem. Solids **2**, 240 (1957).
[18] E. E. Krasovskii, F. Starrost, and W. Schattke, Phys. Rev. B **59**, 10 504 (1999).
[19] W. C. Lee, C. Wu, D. P. Arovas, and S. C. Zhang, Phys. Rev. B **80**, 245439 (2009).
[20] A. S. Núñez and J. Fernández-Rossier, arXiv:1003.5931.